PCCP

Cite this: *Phys. Chem. Chem. Phys.*, 2011, **13**, 19362–19370

www.rsc.org/pccp

PAPER

Quantum instanton calculation of rate constants for the $C_2H_6 + H \rightarrow C_2H_5 + H_2$ reaction: anharmonicity and kinetic isotope effects

Wenji Wang*[a] and Yi Zhao*[b]

Received 11th July 2011, Accepted 6th September 2011
DOI: 10.1039/c1cp22255d

Thermal rate constants and kinetic isotope effects for the title reaction are calculated by using the quantum instanton approximation within the full dimensional Cartesian coordinates. The obtained results are in good agreement with experimental measurements at high temperatures. The detailed investigation reveals that the anharmonicity of the hindered internal rotation motion does not influence the rate too much compared to its harmonic oscillator approximation. However, the motion of the nonreactive methyl group in C_2H_6 significantly enhances the rates compared to its rigid case, which makes conventional reduced-dimensionality calculations a challenge. In addition, the temperature dependence of kinetic isotope effects is also revealed.

1 Introduction

The H + HR → H_2 + R (HR = alkane) reactions[1–4] are interesting for both fundamental research and practical reasons. They are helping to bridge the gap between triatomic and polyatomic reactions, and are also significant steps in the combustion of all alkane compounds. Recently, the reaction

$$\text{(R1)} \quad H + C_2H_6 \rightarrow H_2 + C_2H_5 \qquad (1)$$

has attracted much attention since ethane is the simplest molecule containing a carbon–carbon single bond, and it is also the prototype molecule for hindered internal rotations in a large number of molecules.

The hindered internal rotation about the C–C bond in ethane, complicating the statistical computation, is discovered by Kemp and Pitzer,[5] who showed that only when an internal rotation barrier of about 3 kcal mol^{-1} [6–12] is taken into account could obtain thermodynamic quantities in agreement with experiment. Prior to the calculation of the rates, plenty of work has been done for the investigation of the partition function of a hindered internal rotation.[13–21] In these methods, a key starting point is how to correctly incorporate the contributions from the anharmonicity and vibration–rotational coupling of this internal rotation. Their effects on the partition function may be understood by the comparisons of a free rotor, a hindered rotor, and a harmonic oscillator.[19,22]

Based on these approaches for the partition function, several works have investigated the effect of the hindered internal rotation on the thermal rate constants based on transition state theory (TST). Fernandez-Ramos and Truhlar[23] deal with the internal rotation of the methyl group with respect to the CF_3 group as a hindered rotor. Compared to a harmonic approximation, rate constants are significantly reduced. Vansteenkiste *et al.*[24] use the extended hindered-rotor model (EHR) that properly includes the mode–mode coupling and vibrational–rotational coupling in the treatment of the addition of the vinyl radical to ethene. Compared to the hindered-rotor model (HR), the rate constants are increased. Hennig and Schmatz[25] calculated the quantum dynamics of the $Cl^- + CH_3Br \rightarrow ClCH_3 + Br^-$ reaction, and found that the dynamical inclusion of the rotational degree of freedom leads to a large enhancement in reactivity. These conclusions demonstrate that the vibrational–rotational coupling and anharmonicity from the hindered internal rotation play significant roles in the rate calculations.

For the reaction of H + C_2H_6, there is a hindered internal rotation between two methyl groups (see Fig. 1), making the rate calculation a challenge. In spite of this difficulty, several approximation methods have been used to investigate the rate constants. For instance, Clark and Dove used a simplified form of the bond-energy–bond-order method to calculate rates.[26] Kerkeni and Clary used a reduced-dimensionality quantum dynamics method[27–30] to explicitly consider the torsional and stretching vibrations of C_2H_6, and found that the rates from the two and three degrees of freedom are very similar. Sturdy and Clary[31] applied the Torsional Path Integral Monte Carlo (TPIMC) method to this reaction and found that the rates are halved at room temperature as the torsional anharmonicity is included. Senosiain *et al.*[32] and

[a] *College of Science, Northwest A&F University, Yangling, 712100, Shaanxi Province, P. R. China. E-mail: wjwang@nwsuaf.edu.cn*
[b] *State Key Laboratory for Physical Chemistry of Solid Surfaces and Fujian Provincial Key Lab of Theoretical and Computational Chemistry, College of Chemistry and Chemical Engineering, Xiamen University, Xiamen, 361005, P. R. China. E-mail: yizhao@xmu.edu.cn*

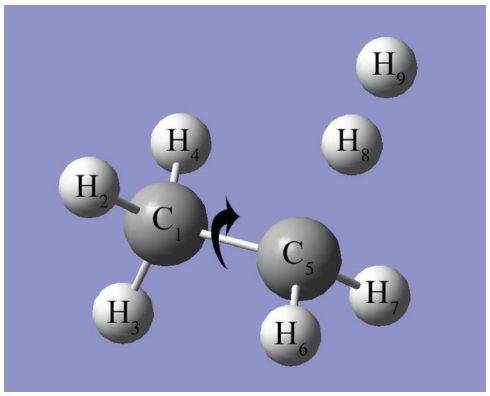

Fig. 1 The geometry for the H + C_2H_6 → H_2 + C_2H_5 reaction at the transition state. It consists of the reactive fragments (labeled as C_5, H_6, H_7, H_8 and H_9) and the nonreactive methyl groups (labeled as C_1, H_2, H_3 and H_4). The nonreactive methyl groups can rotate along the C_1–C_5 bond.

Bryukov *et al.*[33] developed two different methodologies both using quantum chemistry, transition state theory and tunneling corrections to extrapolate experimental data over a broad temperature range. Chakraborty *et al.*[34] calculated the direct dynamics by MPW54 (a modified Perdew–Wang functional with 54% Hartree–Fock exchange). They constructed a CVBMM (a combination of valence bond and molecular mechanics) potential energy surface (PES), and calculated the rates and kinetic isotope effects on this PES with the CVT/SCT (canonical variational transition state theory with the small-curvature tunneling approximation) method in which a hindered rotator approximation is adopted. Layfield *et al.*[35,36] studied this reaction using electronic-structure theory and quasiclassical trajectory calculations evolved with a specific-reaction-parameter semiempirical Hamiltonian.

In the present paper, we use the quantum instanton (QI) approach for the title reaction. The QI method is proposed by Miller *et al.*[37] for the calculations of reaction rates. Its approximation is similar to an earlier semiclassical TST[38] that became known as the instanton model,[39–41] but it has an advantage that the Boltzmann operator is treated fully quantum mechanically rather than within the semiclassical approximation. The QI method does not need to calculate the partition function explicitly, so there is no approximation to the internal rotation, and it can be manipulated in Cartesian space with a full dimensional potential energy surface, thus takes into account the effects of the vibrational–rotational coupling and anharmonicity of the reaction system naturally. In addition, the QI method considers all tunneling paths and automatically gives each path its natural weight by the quantum Boltzmann factor and incorporates the quantum-fluctuation effect correctly. It has been successfully applied to gas phase reactions,[42–45] proton transfer in a polar solvent,[46] surface diffusions[47,48] and kinetic isotope effects.[49–51]

Another objective of the present paper is to consider the contribution of the nonreactive methyl group to the rate constants, as shown in Fig. 1. In the reduced dimensionality calculations,[27,29] several most important degrees of freedom for the reaction are taken into account, with the others fixed. For the title reaction, the role of the degrees of freedom of the nonreactive methyl group in the rate constant is not clear. However, this group may have an important effect on the rates due to its larger steric repulsion in the eclipsed conformation and an enhanced stabilization of the staggered conformation by the hyperconjugation.[7] We therefore investigate the rate change by treating this group rigidly, classically and quantum mechanically, respectively.

In this paper, we also predict the rate constants and kinetic isotope effects (KIEs) for the following reactions with the QI method:

$$\text{(R2)}\quad \mathrm{D} + \mathrm{C_2H_6} \rightarrow \mathrm{HD} + \mathrm{C_2H_5}, \tag{2}$$

$$\text{(R3)}\quad \mathrm{H} + \mathrm{C_2D_6} \rightarrow \mathrm{HD} + \mathrm{C_2D_5}, \tag{3}$$

$$\text{(R4)}\quad \mathrm{D} + \mathrm{C_2D_6} \rightarrow \mathrm{D_2} + \mathrm{C_2D_5}. \tag{4}$$

To the best of our knowledge, there are no experimental investigations on the isotopic reactions of ethane yet. Theoretically, Chakraborty *et al.*[34] showed that the KIE of H + C_2H_6/D + C_2H_6 has a nonmonotonic temperature dependence using the CVT/SCT method. At high temperatures, the KIE increases with increasing temperature, whereas at low temperatures, it decreases with increasing temperature. However, Kerkeni and Clary[28,30] reported that the KIE of H + C_2H_6/D + C_2H_6 always increases with increasing temperature using a reduced-dimensionality quantum dynamical method. We will use the QI method to explore this discrepancy.

The remainder of this paper is as follows: in Section 2 we first summarize the working expression of the QI theory, and then give a detailed description of the title reaction. Computational details are provided in Section 3. Numerical results of the QI rates and the KIEs for the title reaction are presented in Section 4. Section 5 is the conclusion.

2 Quantum instanton theory

2.1 Summary of the quantum instanton theory

In this section, we summarize the work formulas for the QI approximation. The detailed derivation can be found in ref. 37, 42 and 43. The QI model proposes the following thermal rate constant

$$k_{\mathrm{QI}}Q_{\mathrm{r}} \approx \frac{\sqrt{\pi}\hbar}{2}\frac{C_{\mathrm{ff}}(0)}{\Delta H(\beta)}. \tag{5}$$

Here, Q_{r} is the reactant partition function per unit volume. $C_{\mathrm{ff}}(0)$ is the zero time value of the flux–flux correlation function

$$C_{\mathrm{ff}}(t) = \mathrm{tr}[\mathrm{e}^{-\beta\hat{H}/2}\hat{F}_a\mathrm{e}^{-\beta\hat{H}/2}\mathrm{e}^{i\hat{H}t/\hbar}\hat{F}_b\mathrm{e}^{-i\hat{H}t/\hbar}] \tag{6}$$

where β is the inverse temperature ($1/(k_{\mathrm{B}}T)$), $\hat{H}$ is the Hamiltonian operator of the reaction system, and $\hat{F}_a$ and $\hat{F}_b$ are the flux operators, given by

$$\hat{F}_\gamma = \frac{i}{\hbar}[\hat{H}, h(s_\gamma(\hat{\mathbf{r}}))], \tag{7}$$

with $\gamma = a, b$. In eqn (7), h is the step-side function, r represents the Cartesian coordinates of the reaction system, and $s_a(r)$ and $s_b(r)$ define two separate dividing surfaces *via* the

equations $s_a(r) = 0$ and $s_b(r) = 0$, both $s_a(r)$ and $s_b(r)$ being positive (negative) on the product (reactant) side of the dividing surfaces.

ΔH in eqn (5) is a specific type of energy variance, given by

$$\Delta H(\beta) = \hbar\sqrt{\frac{-\ddot{C}_{\rm dd}(0)}{2C_{\rm dd}(0)}}. \quad (8)$$

In order to get the correct free particle (high temperature) limit (that would be 25% too large otherwise), an ad hoc term is added to $\Delta H(\beta)$, $\Delta H_{\rm mod}(\beta) = \Delta H(\beta) + (\sqrt{\pi} - \sqrt{2})/\beta$, which has very little effect on the low temperature regime. $C_{\rm dd}(0)$ and $\ddot{C}_{\rm dd}$ (0) are the zero time value and its second time derivative, respectively, of the "delta–delta" correlation function

$$C_{\rm dd}(t) = {\rm tr}[{\rm e}^{-\beta\hat{H}/2}\Delta(s_a(\hat{\mathbf{r}})){\rm e}^{-\beta\hat{H}/2}{\rm e}^{i\hat{H}t/\hbar}\Delta(s_b(\hat{\mathbf{r}})){\rm e}^{-i\hat{H}t/\hbar}], \quad (9)$$

where the generalized delta-function operator is

$$\Delta(s_\gamma(\hat{\mathbf{r}})) = \delta(s_\gamma(\hat{\mathbf{r}}))\sqrt{\sum_{i=1}^{N}\frac{1}{m_i}(\nabla_i s_\gamma(\hat{\mathbf{r}}))^2}\ (\gamma = a,\ b). \quad (10)$$

Here, N is the total number of atoms, $\nabla_i = \partial/\partial r_i$, r_i denotes the Cartesian coordinates of the ith atom and m_i is its atomic mass.

The dividing surfaces are determined by the stationary condition

$$\frac{\partial}{\partial c_k}C_{\rm dd}(0;\{c_k\}) = 0, \quad (11)$$

where $\{c_k\}$ is a collection of parameters that is involved in the location of the dividing surfaces. This condition originates from the SC instanton model, and the resulting dividing surfaces correspond qualitatively to the turning points of the periodic orbit that runs on an upside down PES in imaginary time.

Since all the relevant quantities in the QI expression (eqn (5)) involved only the quantum Boltzmann operator, they can be readily evaluated using the imaginary time path integral Monte Carlo (PIMC)[52–54] method.

We begin with the simplest quantity, $C_{\rm dd}(0)$, which can be discretized to

$$C_{\rm dd}(0) = C\int{\rm d}r^{(1)}\int{\rm d}r^{(2)}\cdots\int{\rm d}r^{(P)}\Delta(s_a(r^{(0)})) \times\Delta(s_b(r^{(P/2)}))\exp[-\beta\Phi(\{r^{(s)}\})], \quad (12)$$

where C is a multiplicative constant, P the number of imaginary time slices, and $r^{(s)} = (r_1^{(s)}, r_2^{(s)},\ldots, r_N^{(s)})$ the Cartesian coordinates of the system associated with the sth time slice. $\Phi(\{r^{(s)}\})$ is the discretized action given by

$$\Phi(\{r^{(s)}\}) = \frac{P}{2\hbar^2\beta^2}\sum_{s=1}^{P}\sum_{i=1}^{N}m_i(r_i^{(s)} - r_i^{(s-1)})^2 + \frac{1}{P}\sum_{s=1}^{P}V(r^{(s)}), \quad (13)$$

where $r^{(0)} = r^{(P)}$ and $\{r^{(s)}\}$ represents $\{r^{(1)}, r^{(2)},\ldots, r^{(P)}\}$. Path integral expressions for $C_{\rm ff}(0)$ and $\ddot{C}_{\rm dd}(0)$ are somewhat more complicated but can be obtained in a straightforward manner. The appropriate expressions are

$$C_{\rm ff}(0) = C\int{\rm d}r^{(1)}\int{\rm d}r^{(2)}\cdots\int{\rm d}r^{(P)}\Delta(s_a(r^{(0)}))\Delta(s_b(r^{(P/2)})) \times\exp[-\beta\Phi(\{r^{(s)}\})]f_v(\{r^{(s)}\}), \quad (14)$$

with

$$f_v(\{r^{(s)}\}) = \left(\frac{iP}{2\hbar\beta}\right)^2\frac{\sum_{i=1}^{N}\nabla_i s_a(r^{(0)})\cdot(r_i^{(1)} - r_i^{(P-1)})}{\sqrt{\sum_{i=1}^{N}m_i^{-1}(\nabla_i s_a(r^{(0)}))^2}} \times\frac{\sum_{i=1}^{N}\nabla_i s_b(r^{(P/2)})\cdot(r_i^{(P/2+1)} - r_i^{(P/2-1)})}{\sqrt{\sum_{i=1}^{N}m_i^{-1}(\nabla_i s_b(r^{(P/2)}))^2}}, \quad (15)$$

and

$$\ddot{C}_{\rm dd}(0) = \frac{-C}{\hbar^2}\int{\rm d}r^{(1)}\int{\rm d}r^{(2)}\cdots\int{\rm d}r^{(P)}\Delta(s_a(r^{(0)})) \times\Delta(s_b(r^{(P/2)}))\exp[-\beta\Phi(\{r^{(s)}\})] \times\{F(\{r^{(s)}\})^2 + G(\{r^{(s)}\})\}, \quad (16)$$

with

$$F(\{r^{(s)}\}) = -\frac{P}{\hbar^2\beta^2}\left\{\sum_{s=1}^{P/2} - \sum_{s=P/2+1}^{P}\right\}\sum_{i=1}^{N}m_i(r_i^{(s)} - r_i^{(s-1)})^2 + \frac{2}{P}\left\{\sum_{s=1}^{P/2-1} - \sum_{s=P/2+1}^{P-1}\right\}V(r^{(s)}), \quad (17)$$

and

$$G(\{r^{(s)}\}) = \frac{2fP}{\beta^2} - \frac{4P}{\hbar^2\beta^3}\sum_{s=1}^{P}\sum_{i=1}^{N}m_i(r_i^{(s)} - r_i^{(s-1)})^2, \quad (18)$$

with f being the total number of degrees of freedom (*i.e.* $f = 3N$).

In realistic calculations, we rewrite eqn (5) as the product of several ratios

$$k_{\rm QI} = \frac{\sqrt{\pi}\hbar}{2}\frac{C_{\rm dd}(0)}{Q_{\rm r}}\frac{C_{\rm ff}(0)}{C_{\rm dd}(0)}\frac{1}{\Delta H(\beta)}. \quad (19)$$

The terms $C_{\rm ff}(0)/C_{\rm dd}(0)$ and ΔH are directly calculated as a constrained average over the same ensemble of paths.[42,43]

$$C_{\rm ff}(0)/C_{\rm dd}(0) = \langle f_v\rangle, \quad (20)$$

$$\Delta H^2 = \tfrac{1}{2}\langle F^2 + G\rangle, \quad (21)$$

with

$$\langle\cdots\rangle = \frac{\int{\rm d}r^{(1)}\int{\rm d}r^{(2)}\cdots\int{\rm d}r^{(P)}\Delta(s_a(r^{(0)}))\Delta(s_b(r^{(P/2)}))\exp[-\beta\Phi(\{r^{(s)}\})](\cdots)}{\int{\rm d}r^{(1)}\int{\rm d}r^{(2)}\cdots\int{\rm d}r^{(P)}\Delta(s_a(r^{(0)}))\Delta(s_b(r^{(P/2)}))\exp[-\beta\Phi(\{r^{(s)}\})]}. \quad (22)$$

The evaluation of $C_{\rm dd}(0)/Q_{\rm r}$, however, meets a challenge because $C_{\rm dd}(0)$ is the quantity associated with the transition

state, while Q_r with the asymptotic reactant domain, the detailed treatment of this factor will be described in the next section.

2.2 Application to the gas phase H + C_2H_6 reaction

We now apply the QI model to the hydrogen abstraction reaction from ethane by a hydrogen atom (R1), Fig. 1 shows the transition state geometry for the title reaction. The Hamiltonian operator $\hat{H}$ for this system in three-dimensional space is

$$\hat{H} = \sum_{i=1}^{9} \frac{\hat{\mathbf{p}}_i^2}{2m_i} + V(\hat{\mathbf{r}}_1, \hat{\mathbf{r}}_2, \ldots, \hat{\mathbf{r}}_9), \quad (23)$$

where the coordinate operators, masses and momentum operators corresponding to the ith atom are denoted with $\hat{\mathbf{r}}_i$, m_i, and $\hat{\mathbf{p}}_i$ respectively. The CVBMM (a combination of valence bond functional forms for the reactive fragments (C_5, H_6, H_7, H_8, H_9) and a molecular mechanics potential for the nonreactive parts (C_1, H_2, H_3, H_4)) potential energy surface constructed by Chakraborty *et al.*[34] is employed in our calculations. The CVBMM PES is available in POTLIB.[55]

To proceed further, it is necessary to define a generalized reaction coordinate $s(r; \xi)$, where ξ is an adjustable parameter that shifts the location of the dividing surface (defined by $s(r; \xi) = 0$). The essential strategy for defining $s(r; \xi)$ is the same as that described in ref. 43, *i.e.*, $s(r; \xi)$ is defined by a linear interpolation between two constituent reaction coordinates $s_0(r)$ and $s_1(r)$ through the parameter ξ,

$$s(r; \xi) = \xi s_1(r) + (1 - \xi)s_0(r), \quad (24)$$

$s_1(r)$ is a reaction coordinate whose dividing surface is designed to pass through the top of the classical potential barrier, which is defined here as

$$s_1(r) = \max[s_1^6(r), s_1^7(r), s_1^8(r)] \quad (25)$$

with $s_1^x(r)$ ($x = 6, 7, 8$) being

$$s_1^x(r) = r(C_5\text{–}H_x) - r(H_x\text{–}H_9) - [r^{\ddagger}(C_5\text{–}H_x) - r^{\ddagger}(H_x\text{–}H_9)], \quad (26)$$

where r(X–Y) denotes the interatomic distance between atoms X and Y and $r^{\ddagger}$(X–Y) is the value at the transition state geometry. It should be noted that we only consider the reactions of H_9 with H_6, H_7 and H_8 in $s_1^x(r)$. However, the total rates of H + C_2H_6 are two times as large as our calculated results (in this paper, all the tabulated rates are the total ones). $s_0(r)$ in eqn (24), on the other hand, describes a dividing surface that is located far in the asymptotic reactant valley, which is given by

$$s_0(r) = R_\infty - |R|. \quad (27)$$

Here R is the scattering vector that connects the incident hydrogen and the center of mass of the ethane. R_∞ is an adjustable parameter which is chosen to be 10 Å in order to guarantee that the interaction potential energy between H and C_2H_6 is negligible. In this case, the dividing surfaces are only related to one parameter ξ with $s(r; 0) = s_0(r)$ and $s(r; 1) = s_1(r)$. The dividing surface moves smoothly from the asymptotic reactant domain to the transition state region when ξ changes from 0 to 1. $C_{dd}(0)$ (in eqn (19)) now becomes a function of two parameters (ξ_a, ξ_b)[42,43]

$$C_{dd}(0; \xi_a, \xi_b) = \mathrm{tr}[e^{-\beta\hat{H}/2}\Delta(s(\hat{\mathbf{r}}, \xi_a))e^{-\beta\hat{H}/2}\Delta(s(\hat{\mathbf{r}}, \xi_b))]. \quad (28)$$

It is easy to see from eqn (11) that the condition of locating the dividing surfaces becomes

$$\frac{\partial C_{dd}(0; \xi_a, \xi_b)}{\partial \xi_a} = 0, \quad \frac{\partial C_{dd}(0; \xi_a, \xi_b)}{\partial \xi_b} = 0. \quad (29)$$

In this case, locating the two optimized dividing surfaces is switched to finding the two optimized parameters (ξ_a, ξ_b).

As it has been shown,[42] if $\xi_a = \xi_b = 0$, the ratio of $C_{dd}(0; 0,0)/Q_r$ becomes

$$\frac{C_{dd}(0; 0, 0)}{Q_r} = \left[\frac{\mu_R}{2\pi\hbar^2\beta}\right]^{-3/2} C_{dd}^{trans}(0), \quad (30)$$

with

$$C_{dd}^{trans}(0) = \mathrm{tr}[e^{-\beta\hat{T}_R/2}\Delta(R_\infty - |\hat{R}|)e^{-\beta\hat{T}_R/2}\Delta(R_\infty - |\hat{R}|)], \quad (31)$$

where $\hat{T}_R = \hat{P}_R^2/2\mu_R$, μ_R is the reduced mass of two reactants. The value of eqn (31) involves the contribution from the translation motion of the two reactants, and it can be derived into an analytical form,[43] that leads to

$$\frac{C_{dd}(0; 0, 0)}{Q_r} = \frac{4R_\infty^2}{\hbar}\left(\frac{2\pi}{\mu_R\beta}\right)^{1/2}. \quad (32)$$

The advantage of eqn (32) is that it allows the numerical simulation to circumvent the problem of accurately evaluating the partition functions of reactants.

Finally, the ratio $C_{dd}(0)/Q_r$ in eqn (19) can be written as

$$\frac{C_{dd}(0; \xi_a, \xi_b)}{Q_r} = \frac{C_{dd}(0; 0, 0)}{Q_r} \times \frac{C_{dd}(0; \xi_a, \xi_b)}{C_{dd}(0; 0, 0)}, \quad (33)$$

where the first ratio is given by eqn (32), and the second one can be handled *via* the available adaptive umbrella sampling techniques.[56–58]

The free energy curve can be defined by

$$F(\xi) = -k_B T \log[C_{dd}(0; \xi_a, \xi_b)], \quad (34)$$

where $\xi = \xi_a - \xi_b$.

3 Computational details

In path integral calculations, the sampling of the discrete paths is performed with the Monte Carlo method. For the atoms treated quantum mechanically, the numbers of time slice, P, are chosen to be 20 and 120 at temperatures 1000 K and 200 K, respectively. For the ones treated classically, the numbers of time slice are always set to be 1. The number of Monte Carlo cycle is about $6 \times 10^6 - 4 \times 10^7$ for computing a single ensemble average. It converges most of the values within 10% statistical errors.

4 Results and discussions

4.1 Reaction rates of H + C_2H_6

We calculate the reaction rates of H + C_2H_6 on the CVBMM PES with all the atoms treated quantum mechanically.

Table 1 Rate constants for the H + C_2H_6 reaction[a]

T/K	Present QI	CVT/SCT[b]	Quantum 2D[c]	Expt.[d]	Expt.[e]	Expt.[f]	Expt.[g]
200	1.16(−18)	1.90(−18)	4.08(−21)				
281					1.40(−17)		
295					2.54(−17)		
300	1.15(−16)	1.44(−16)					
316					6.11(−17)		
320			2.36(−17)				
347					1.70(−16)		
385						1.01(−15)	
400	2.73(−15)	2.40(−15)					
417						1.76(−15)	
420			9.08(−16)				
475						8.79(−15)	
491		1.45(−14)		1.42(−14)			
500	1.96(−14)						
503							2.16(−14)
520			9.43(−15)				
544						4.39(−14)	
583							8.31(−14)
586		5.89(−14)		5.45(−14)			
600	8.43(−14)	7.03(−14)					
680			1.06(−13)				
683							2.41(−13)
693		1.98(−13)		2.21(−13)			
700	2.68(−13)						
703							3.16(−13)
796		4.97(−13)		4.45(−13)			
800	6.53(−13)						
880			7.12(−13)				
1000	2.45(−12)	1.96(−12)	1.61(−12)				

[a] Unit: $cm^3\ s^{-1}$, powers of 10 are in parentheses. [b] From ref. 34. [c] From ref. 27. [d] From ref. 33. [e] From ref. 59. [f] From ref. 60. [g] From ref. 61.

In Table 1, we summarize the present QI rates and the CVT/SCT values reported by Chakraborty *et al.*,[34] as well as the quantum 2D ones calculated by Kerkeni and Clary.[27] We also include some experimental data[33,59–61] in Table 1. The corresponding Arrhenius plots are displayed in Fig. 2. It is seen that the QI results and the CVT/SCT ones have slightly different Arrhenius curves, where the QI curve is a little higher at high temperatures but lower at low temperatures. The QI rate is smaller than the CVT/SCT one by 39% at 200 K, we think that this discrepancy is due to the overestimation of the tunneling effect by the CVT/SCT method, since the CVT/SCT method uses an optimized tunneling path while the QI method considers all tunneling paths and automatically gives each path its natural weight by the quantum Boltzmann factor. The results of the two-dimensional quantum dynamics are much smaller than both the QI and the CVT/SCT ones throughout the temperature range considered in the present study. This is because a higher vibrational adiabatic barrier (12.0 kcal mol^{-1}, while it is 9.95 kcal mol^{-1} for the CVBMM PES) is used in the quantum 2D calculations. In Fig. 2, we can also see that the QI results are in good agreement with the experimental data at high temperatures, however, they are much larger than the experimental ones at low temperatures. To clarify this discrepancy, a more exact potential energy surface or more reliable experimental data may be needed.

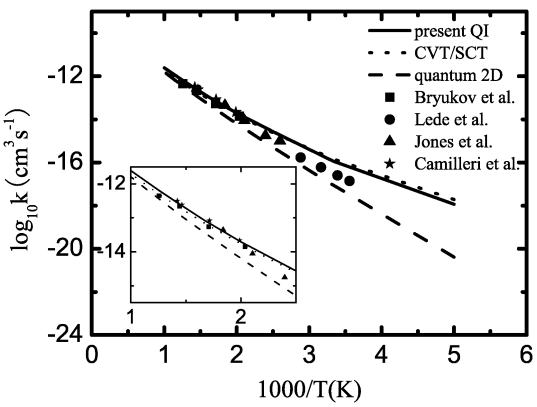

Fig. 2 Arrhenius plots of the thermal rate constants for the H + C_2H_6 reaction. Solid line: the present QI results; dotted line: the CVT/SCT results from ref. 34; dashed line: the two-dimensional quantum dynamical values;[27] filled squares, circles, triangles and stars are corresponding to the experimental values of Bryukov *et al.*,[33] Lede *et al.*,[59] Jones *et al.*[60] and Camilleri *et al.*,[61] respectively.

4.2 Effect of the hindered internal rotation

In this section, we treat the internal rotation of the title reaction as a harmonic oscillator, so as to investigate the sole contribution of the hindered internal rotation to the rates. Here, a harmonic oscillator approximation means that the internal rotation is restricted, just as it has an infinite rotation barrier. A detailed computational strategy is showed in Fig. 3, where the geometry of the title reaction at the transition state, three special planes (Plane-a, Plane-b and Plane-c) and three special regions (A, B and C) are displayed. In Fig. 3, 'Plane-a', 'Plane-b' and 'Plane-c' stand for the planes of H_2–C_1–C_5 (the C_5 atom is just behind the C_1 atom, as seen in Fig. 1),

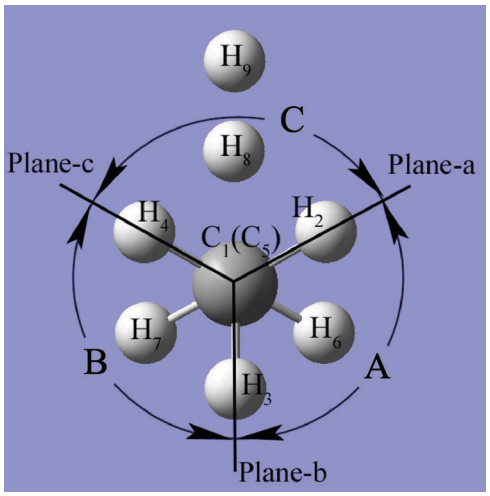

Fig. 3 The space is divided into three parts (A, B and C) by three planes (Plane-a, Plane-b and Plane-c) at the transition state geometry of the title reaction. 'Plane-a', 'Plane-b' and 'Plane-c' denote the planes of H_2–C_1–C_5 (the C_5 atom is just behind the C_1 atom, as seen in Fig. 1), H_3–C_1–C_5 and H_4–C_1–C_5, respectively. The space between 'Plane-a' and 'Plane-b' is labeled as 'A'; the space between 'Plane-b' and 'Plane-c' is labeled as 'B'; the space between 'Plane-a' and 'Plane-c' is labeled as 'C'. The movements of H_6, H_7 and H_8 atom are restricted within the regions of 'A', 'B' and 'C', respectively.

H_3–C_1–C_5 and H_4–C_1–C_5, respectively. The space between 'Plane-a' and 'Plane-b' is labeled as 'A'; the space between 'Plane-b' and 'Plane-c' is labeled as 'B'; the space between 'Plane-a' and 'Plane-c' is labeled as 'C'. In the calculations, the movements of H_6, H_7 and H_8 atoms are restricted within the regions 'A', 'B' and 'C', respectively. The calculated results for the H + C_2H_6 reaction are tabulated in Table 2, where k_{QI} and k_{QI}^{HO} denote the QI rates and the QI rates with a harmonic oscillator approximation to the internal rotation. Their ratios (k_{QI}^{HO}/k_{QI}) are also included in Table 2. We also listed the values of CVT/SCT[34] (the lowest-frequency mode is treated as a harmonic oscillator and a hindered rotator, respectively) and TPIMC[31] (the internal rotation is treated as a harmonic oscillator and an anharmonic torsion, respectively) in Table 2.

In Table 2, we can see that the values of k_{QI}^{HO}/k_{QI} decrease with increasing temperature. Our ratios are close to 1 in the tested temperature range. The detailed analysis manifests that both the partition functions of the reactant and transition state involve an internal rotation and their changes from the anharmonicity are cancelled because of $k_{QI}^{HO}/k_{QI} \propto (Q_{ts}^{HO}Q_r)/(Q_r^{HO}Q_{ts})$, though the partition function for the hindered internal rotation is bigger than that of a harmonic oscillator.[31] To be concrete, the ratios of QI are bigger than 1 at low temperatures, which is caused by the fact that the reactant partition function grows faster than the transition state partition function when the internal rotation is treated from a harmonic approximation to a hindered internal rotation. However, these enhancements are opposite at high temperatures, leading to the ratio smaller than 1.

It is interesting to note that the ratios from the CVT/SCT are always equal to 1.1. It is consistent with the QI result at low temperatures. At high temperatures, however, the QI ratios are smaller. This may be explained by the vibrational–rotational coupling, which can enhance the rates at high temperature, consistent with a previous work.[24] For the TPIMC results, the tendency of temperature dependence is the same as the QI data, but the ratios are nearly two times larger than QI results.

4.3 Roles of the nonreactive methyl group

It is expected that the motion of the nonreactive methyl group may have an effect on the hydrogen abstraction rates. To reveal this property, we calculate the rate by treating the nonreactive methyl group rigidly, classically and quantum mechanically, respectively. For the rigid group, three bonds (C_1–H_2, C_1–H_3 and C_1–H_4) and three angles ($\angle H_2$–C_1–H_3, $\angle H_3$–C_1–H_4 and $\angle H_2$–C_1–H_4) are fixed, as shown in Fig. 1. In the classical calculation, we take the time slice in the path integral to be one for the atoms in the group. It should be mentioned that all the atoms of the reactive fragments are always treated quantum mechanically and the internal rotation is not restricted.

Table 3 displays the three kinds of rates (k_{QI}^{q}, k_{QI}^{c} and k_{QI}^{r}) for the four isotopic reactions (R1–R4). Here, k_{QI}^{q} is the rate that all the nine atoms are treated quantum mechanically. k_{QI}^{c} represents the value that the nonreactive methyl group is treated classically. k_{QI}^{r} corresponds to the one that the nonreactive methyl group is treated rigidly. Table 3 clearly shows that k_{QI}^{q} is always the biggest while k_{QI}^{r} is always the smallest in the tested temperature range. More detailed comparisons of k_{QI}^{q} with k_{QI}^{c} and k_{QI}^{r} are displayed in Fig. 4. The values of k_{QI}^{q}/k_{QI}^{c} and k_{QI}^{q}/k_{QI}^{r} for the four isotopic reactions are all bigger than 1 and decrease with increasing temperature. It manifests that the rates from quantum nonreactive groups are always greater than those from the classical and rigid groups. Meanwhile, Fig. 4 also shows that classical rates are greater than the rigid rates. At low temperature, for instance, at 200 K, the quantum rate can be 5 times greater than the rigid one.

Table 2 Two kinds of QI rates and their ratios for the title reaction[a]

T/K	180	200	250	300	400	700	1000	1100
k_{QI}	3.59(−19)	1.16(−18)	1.40(−17)	1.15(−16)	2.73(−15)	2.68(−13)	2.45(−12)	
k_{QI}^{HO}	4.40(−19)	1.38(−18)	1.57(−17)	1.17(−16)	2.68(−15)	2.45(−13)	2.20(−12)	
k_{QI}^{HO}/k_{QI}[b]	1.23	1.19	1.12	1.02	0.98	0.91	0.90	
CVT/SCT[c]		1.1		1.1	1.1	1.1	1.1	
TPIMC[d]				2.02		1.55		1.42

[a] Unit: $cm^3\ s^{-1}$, powers of 10 are in parentheses. [b] k_{QI} and k_{QI}^{HO} denote the QI rates and the QI rates with a harmonic oscillator approximation to the internal rotation. [c] From ref. 34. [d] From ref. 31.

Table 3 The rates[a] for the four isotopic reactions (R1–R4)

T/K		H + C_2H_6	D + C_2H_6	H + C_2D_6	D + C_2D_6
200	k^q_{QI}	1.16(−18)	3.11(−18)	6.27(−21)	1.27(−20)
	k^c_{QI}	4.51(−19)	1.10(−18)	2.96(−21)	6.90(−21)
	k^r_{QI}	2.87(−19)	6.26(−19)	1.66(−21)	4.68(−21)
300	k^q_{QI}	1.15(−16)	2.23(−16)	4.92(−18)	9.77(−18)
	k^c_{QI}	5.68(−17)	1.01(−16)	2.69(−18)	6.18(−18)
	k^r_{QI}	3.64(−17)	6.74(−17)	1.91(−18)	4.54(−18)
400	k^q_{QI}	2.73(−15)	3.98(−15)	2.97(−16)	3.98(−16)
	k^c_{QI}	1.52(−15)	2.28(−15)	1.84(−16)	2.97(−16)
	k^r_{QI}	1.09(−15)	1.59(−15)	1.43(−16)	2.06(−16)
500	k^q_{QI}	1.96(−14)	2.64(−14)	3.61(−15)	4.47(−15)
	k^c_{QI}	1.19(−14)	1.58(−14)	2.62(−15)	3.62(−15)
	k^r_{QI}	9.29(−15)	1.19(−14)	2.00(−15)	2.52(−15)
600	k^q_{QI}	8.43(−14)	9.80(−14)	2.29(−14)	2.49(−14)
	k^c_{QI}	5.75(−14)	6.71(−14)	1.78(−14)	2.11(−14)
	k^r_{QI}	4.45(−14)	5.58(−14)	1.40(−14)	1.47(−14)
700	k^q_{QI}	2.68(−13)	2.89(−13)	1.01(−13)	9.79(−14)
	k^c_{QI}	2.13(−13)	2.11(−13)	8.12(−14)	8.76(−14)
	k^r_{QI}	1.52(−13)	1.77(−13)	6.52(−14)	6.29(−14)
800	k^q_{QI}	6.53(−13)	6.68(−13)	2.96(−13)	2.77(−13)
	k^c_{QI}	5.44(−13)	5.09(−13)	2.44(−13)	2.54(−13)
	k^r_{QI}	4.17(−13)	4.31(−13)	1.99(−13)	1.87(−13)
1000	k^q_{QI}	2.45(−12)	2.44(−12)	1.35(−12)	1.30(−12)
	k^c_{QI}	2.20(−12)	2.21(−12)	1.26(−12)	1.26(−12)
	k^r_{QI}	1.70(−12)	1.81(−12)	1.00(−12)	9.54(−13)

[a] Unit: $cm^3\ s^{-1}$, powers of 10 are in parentheses. k^q_{QI}, k^c_{QI} and k^r_{QI} are the rates that the nonreactive methyl group is treated quantum mechanically, classically and rigidly, respectively.

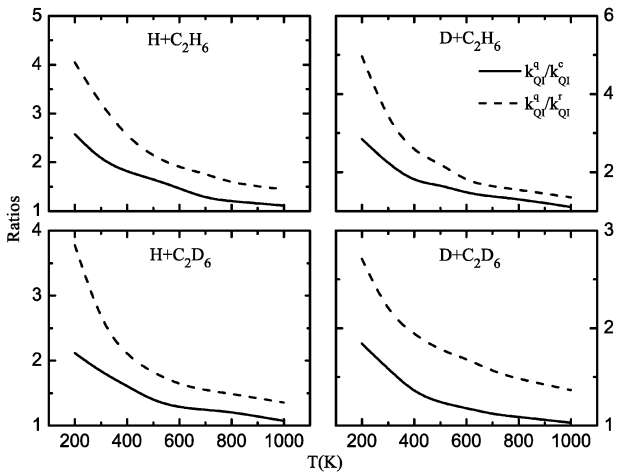

Fig. 4 The values of k^q_{QI}/k^c_{QI} and k^q_{QI}/k^r_{QI} for the four isotopic reactions at different temperatures. k^q_{QI}, k^c_{QI} and k^r_{QI} are the rates that the nonreactive methyl group is treated quantum mechanically, classically and rigidly, respectively.

To find the reason for these differences, we plot in Fig. 5 the free energy profiles for the H + C_2H_6 reaction at 200 K and 1000 K, respectively. It is clearly shown that the quantum effect lowers the free energy barrier, which can be explained by the enhanced hyperconjugation from the delocalizations of the H and C atoms[7,62] to stabilize the transition state much more than the reactant. Whereas, the rigid group always increases the free energy barrier compared to the quantum and classical groups.

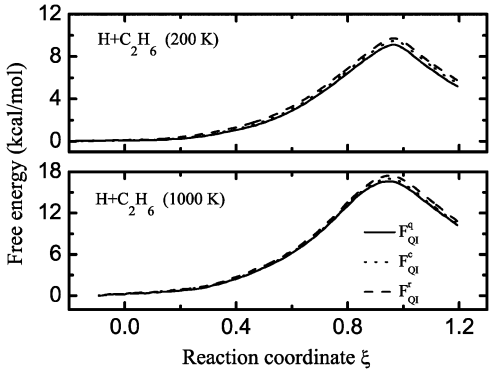

Fig. 5 Free energy profiles for the H + C_2H_6 reaction along the reaction coordinate at 200 and 1000 K. F^q_{QI}, F^c_{QI} and F^r_{QI} denote the free energies that the nonreactive methyl group is treated quantum mechanically, classically and rigidly, respectively.

At high temperatures, the values of k^q_{QI}/k^c_{QI} are close to 1, indicating that the quantum effect becomes weak, as expected. However, the values of k^q_{QI}/k^r_{QI} are still bigger than 1, because of the larger barrier from the rigid group, as shown in Fig. 5.

We thus conclude that the nonreactive methyl group plays an important role in the hydrogen abstraction reaction. Compared to the rigid nonreactive methyl group, the quantized nonreactive methyl group can enhance the rates by several times at low temperatures.

4.4 Kinetic isotope effects

The kinetic isotope effect (KIE) is defined as the ratio k_i/k_j, where k_i is the rate constant for the isotopic reaction with lighter mass, and k_j is the rate constant for the corresponding heavier isotopic reaction. The KIEs calculated by the QI method, the CVT/SCT method[34] and the quantum 2D method[28] are tabulated in Table 4. Compared to the quantum 2D results, the KIEs (R1/R2) from the QI and CVT/SCT are much larger, and those from CVT/SCT have an opposite temperature dependence at low temperatures. These situations come from the different potential energy surface used in the quantum 2D calculation. The previous investigations[63,64] show that opposite temperature dependences are obtained on two different potential energy surfaces even with the same dynamical method. Therefore, we only focus on the comparison between the QI and CVT/SCT results. For the KIE (R1/R2), KIE (R1/R3) and KIE (R1/R4), the QI predicts similar values to the CVT/SCT at high temperatures. However, the explicit differences occur at low temperatures. The QI gives out two times larger KIE (R1/R4) at 200 K. Especially for the KIE (R1/R2), the QI shows that the values monotonically increase with increasing temperature while the CVT/SCT predicts a nonmonotonic temperature dependence. Chakraborty *et al.*[34] explained this nonmonotonic property by the different temperature dependences of the quasi-symmetric stretch mode of the forming and breaking bond and the tunneling contribution. The present QI calculation manifests that this nonmonotonic behavior may come from the overestimation of the tunneling contribution in the CVT/SCT approach, as shown in Section 4.1.

Table 4 The kinetic isotope effects (KIEs) at different temperatures

	KIE (R1/R2)			KIE (R1/R3)		KIE (R1/R4)	
T/K	QI	CVT/SCT[a]	Quantum 2D[b]	QI	CVT/SCT	QI	CVT/SCT
200	0.37	0.69	2.06(−3)	185	173	91.5	40.1
250		0.56					
300	0.52	0.55	2.75(−2)	23.6	24.6	11.8	8.81
400	0.69	0.60	8.24(−2)	9.22	8.92	6.88	4.51
491		0.66			5.28		3.22
500	0.74		0.15	5.43		4.39	
600	0.86	0.73	0.22	3.69	3.59	3.39	2.51
700	0.93		0.29	2.66		2.74	
800	0.98		0.35	2.21		2.36	
1000	1.00	0.79	0.46	1.81	1.94	1.88	1.86

[a] From ref. 34. [b] From ref. 28.

5 Concluding remarks

We have evaluated the rates and kinetic isotope effects for the $H + C_2H_6 \rightarrow H_2 + C_2H_5$ reaction on the CVBMM potential energy surface using the quantum instanton approximation (QI). The calculated rates are in good agreement with experimental data at high temperatures. Compared to the rates predicted by the canonical variational transition state theory with the small-curvature tunneling approximation (CVT/SCT), the QI results have a slightly different Arrhenius curve, where the QI results are a little higher at high temperatures but lower at low temperatures. The QI rate at 200 K is smaller than the CVT/SCT one by 39%. This may be explained by the overestimation of the tunneling effect in the CVT/SCT method.

The detailed investigation reveals that the harmonic oscillator approximation for the internal rotation in the title reaction does not change the rates too much, however, it tends to enhance the rates at low temperatures and lower the rates at high temperatures. We have also investigated the effect of the motion of the nonreactive methyl group on the rates. It is found that the rigid nonreactive methyl group always predicts the smaller rates compared to the quantum one, especially, the rigid group can lead to 5 times smaller rate at 200 K, which makes the reduced-dimensionality calculation a challenge.

Acknowledgements

This work has been supported by the Scientific Research Foundation of Northwest A&F University (Grant No. Z109021103), and the National Science Foundation of China (Grant No. 20833004 and 21073146). The research is supported by high-performance computing platform of Northwest A&F University.

References

1 A. Teslja and J. J. Valentini, *J. Chem. Phys.*, 2006, **125**, 132304.
2 A. J. C. Varandas, P. J. S. B. Caridade, J. Z. H. Zhang, Q. Cui and K. L. Han, *J. Chem. Phys.*, 2006, **125**, 064312.
3 E. Ranzi, M. Dente, T. Faravelli and G. Pennati, *Combust. Sci. Technol.*, 1994, **95**, 1.
4 D. L. Baulch, C. T. Bowman, C. J. Cobos, R. A. Cox, Th. Just, J. A. Keer, M. J. Pilling, D. Stocker, J. Troe, W. Tsang, R. W. Walker and J. Warnatz, *J. Phys. Chem. Ref. Data*, 2005, **34**, 757.
5 J. D. Kemp and K. S. Pitzer, *J. Chem. Phys.*, 1936, **4**, 749.
6 G. Ercolani, *J. Chem. Educ.*, 2005, **82**, 1703.
7 D. Asturiol, P. Salvador and I. Mayer, *ChemPhysChem*, 2009, **10**, 1987.
8 Y. Mo and J. Gao, *Acc. Chem. Res.*, 2007, **40**, 113.
9 P. R. Schreiner, *Angew. Chem., Int. Ed.*, 2002, **41**, 3579.
10 V. Pophristic and L. Goodman, *Nature*, 2001, **411**, 565.
11 R. M. Pitzer, *Acc. Chem. Res.*, 1983, **16**, 207.
12 S. Liu and N. Govind, *J. Phys. Chem. A*, 2008, **112**, 6690.
13 K. S. Pitzer and W. D. Gwinn, *J. Chem. Phys.*, 1942, **10**, 428.
14 K. S. Pitzer, *J. Chem. Phys.*, 1946, **14**, 239.
15 J. E. Kilpatrick and K. S. Pitzer, *J. Chem. Phys.*, 1949, **17**, 1064.
16 J. C. M. Li and K. S. Pitzer, *J. Phys. Chem.*, 1956, **60**, 466.
17 D. G. Truhlar, *J. Comput. Chem.*, 1991, **12**, 266.
18 R. B. Mcclurg, R. C. Flagan and W. A. Goddard III, *J. Chem. Phys.*, 1997, **106**, 6675.
19 P. Y. Ayala and H. B. Schlegel, *J. Chem. Phys.*, 1998, **108**, 2314.
20 J. Pfaendtner, X. Yu and L. J. Broadbelt, *Theor. Chem. Acc.*, 2007, **881**, 118.
21 J. Zheng, T. Yu, E. Papajak, I. M. Alecu, S. L. Mielke and D. G. Truhlar, *Phys. Chem. Chem. Phys.*, 2011, **13**, 10885.
22 A. L. L. East and L. Radom, *J. Chem. Phys.*, 1997, **106**, 6655.
23 A. Fernandez-Ramos and D. G. Truhlar, *J. Chem. Theory Comput.*, 2005, **1**, 1063.
24 P. Vansteenkiste, D. V. Neck, V. V. Speybroeck and M. Waroquier, *J. Chem. Phys.*, 2006, **124**, 044314.
25 C. Hennig and S. Schmatz, *J. Chem. Phys.*, 2009, **131**, 224303.
26 T. C. Clark and J. E. Dove, *Can. J. Chem.*, 1973, **51**, 2147.
27 B. Kerkeni and D. C. Clary, *J. Chem. Phys.*, 2004, **121**, 6809.
28 B. Kerkeni and D. C. Clary, *J. Phys. Chem. A*, 2004, **108**, 8966.
29 B. Kerkeni and D. C. Clary, *J. Chem. Phys.*, 2005, **123**, 064305.
30 B. Kerkeni and D. C. Clary, *Phys. Chem. Chem. Phys.*, 2006, **8**, 917.
31 Y. K. Sturdy and D. C. Clary, *Phys. Chem. Chem. Phys.*, 2007, **9**, 2397.
32 J. P. Senosiain, C. B. Musgrave and D. M. Golden, *J. Phys. Chem. A*, 2001, **105**, 1669.
33 M. G. Bryukov, I. R. Slagle and V. D. Knyazev, *J. Phys. Chem. A*, 2001, **105**, 6900.
34 A. Chakraborty, Y. Zhao, H. Lin and D. G. Truhlar, *J. Chem. Phys.*, 2006, **124**, 044315.
35 J. P. Layfield, M. D. Owens and D. Troya, *J. Chem. Phys.*, 2008, **128**, 194302.
36 J. P. Layfield and D. Troya, *Chem. Phys. Lett.*, 2009, **467**, 243.
37 W. H. Miller, Y. Zhao, M. Ceotto and S. Yang, *J. Chem. Phys.*, 2003, **119**, 1329.
38 W. H. Miller, *J. Chem. Phys.*, 1975, **62**, 1899.
39 S. Coleman, *Phys. Rev. D: Part. Fields*, 1977, **15**, 2929.
40 M. Kryvohuz, *J. Chem. Phys.*, 2011, **134**, 114103.
41 S. C. Althorpe, *J. Chem. Phys.*, 2011, **134**, 114104.
42 T. Yamamoto and W. H. Miller, *J. Chem. Phys.*, 2004, **120**, 3086.
43 Y. Zhao, T. Yamamoto and W. H. Miller, *J. Chem. Phys.*, 2004, **120**, 3100.
44 W. Wang, S. Feng and Y. Zhao, *J. Chem. Phys.*, 2007, **126**, 114307.
45 M. Buchowiecki and J. Vanicek, *J. Chem. Phys.*, 2010, **132**, 194106.
46 T. Yamamoto and W. H. Miller, *J. Chem. Phys.*, 2005, **122**, 044106.

47 W. Wang and Y. Zhao, *J. Chem. Phys.*, 2009, **130**, 114708.
48 W. Wang and Y. Zhao, *J. Chem. Phys.*, 2010, **132**, 064502.
49 J. Vanicek, W. H. Miller, J. F. Castillo and F. J. Aoiz, *J. Chem. Phys.*, 2005, **123**, 054108.
50 J. Vanicek and W. H. Miller, *J. Chem. Phys.*, 2007, **127**, 114309.
51 T. Zimmermann and J. Vanicek, *J. Chem. Phys.*, 2009, **131**, 024111.
52 B. J. Berne and D. Thirumalai, *Annu. Rev. Phys. Chem.*, 1986, **37**, 401.
53 D. M. Ceperley, *Rev. Mod. Phys.*, 1995, **67**, 279.
54 C. Chakravarty, *Int. Rev. Phys. Chem.*, 1997, **16**, 421.
55 R. J. Duchovic, Y. L. Volobuev, G. C. Lynch, A. W. Jasper, D. G. Truhlar, T. C. Allison, A. F. Wagner, B. C. Garrett, J. Espinosa-Garcia and J. C. Corchado, POTLIB online: http://comp.chem.umn.edu/potlib.
56 M. Mezei, *J. Comput. Phys.*, 1987, **68**, 237.
57 R. W. W. Hooft, B. P. V. Eijck and J. Kroon, *J. Chem. Phys.*, 1992, **97**, 6690.
58 C. Bartels and M. Karplus, *J. Comput. Chem.*, 1997, **18**, 1450.
59 J. Lede and J. Villermaux, *Can. J. Chem.*, 1978, **56**, 392.
60 D. Jones, P. A. Morgan and J. H. Purnell, *J. Chem. Soc., Faraday Trans. 1*, 1977, **73**, 1311.
61 P. Camilleri, R. M. Marshall and J. H. Purnell, *J. Chem. Soc., Faraday Trans. 1*, 1974, **70**, 1434.
62 R. S. Mulliken, *J. Chem. Phys.*, 1939, **7**, 339.
63 J. Espinosa-Garcia, J. Sanson and J. C. Corchado, *J. Chem. Phys.*, 1998, **109**, 466.
64 J. Cao, Z. Zhang, C. Zhang, W. Bian and Y. Guo, *J. Chem. Phys.*, 2011, **134**, 024315.

